Effect of Zinc Content and Cutting Tool Coating on the Machinability of the Al-(5–35) Zn Alloys

Şenol Bayraktar[1] · Ali Paşa Hekimoğlu[1]

Abstract

In this study, Al-5Zn, Al-15Zn, Al-25Zn and Al-35Zn alloys containing 5, 15, 25 and 35 wt% Zn, respectively were produced by permanent mold casting. Their microstructures and mechanical properties were investigated using metallography and universal hardness and tensile tests. Cutting tests of the alloys produced were carried out in a vertical machining center. During the tests, the cutting forces were continuously measured and saved by a software. The roughness of the machined surfaces of the alloy samples was measured accordance with the standard of ISO 4287. It was observed that Al-(5–15)Zn alloys exhibit single phase (aluminum rich α) microstructure while Al-(25–35)Zn alloys exhibit two-phase microstructure consisting of α and zinc rich η. As the zinc content increased the hardness and tensile strength of the alloys increased, but their elongation to fracture decreased. Cutting force, surface roughness, formation of built-up edge (BUE) and built-up layer (BUL), and the size of the chip occurring in the machining of the alloys decreased with increasing zinc content. The machining of the Al-(5-35)Zn alloys with uncoated WC tools results in both lower cutting forces and better surface quality compared to titanium-aluminum-nitride (TiAlN) coated tools. The changes in the cutting properties of the tested alloys with the increasing zinc content were discussed in the based on changes in structural and mechanical properties.

1 Introduction

Aluminum (Al) based alloys are preferred in automotive and aerospace industries due to their advantages such as low density and high specific strength [1]. Despite these advantages, in order to improve their mechanical and tribological properties which are insufficient for some applications and/or to extend their usage areas [2], extensive research and development studies have been carried out on Al-based alloys in recent years [3]. In these studies, it was observed that the addition of different alloying elements significantly improved the mechanical and/or tribological properties of Al-based alloys. Zinc (Zn) is one of the alloying elements commonly used in aluminum alloys. It is revealed that Zn additions significantly increase the hardness and strength values of aluminum based alloys with the solid solution and/or secondary phase hardening mechanisms [4–6]. Solid solution hardening is caused by the distortion of the lattice structure because the size of the Zn atoms dissolved in Al is different from the Al atoms. The distortion in the lattice structure causes an increase in strength of the material as it makes the movement of the dislocations difficult. In the secondary phase hardening mechanism, the hardness and strength values increase due to the internal stresses caused by the formation of the new phase in the matrix. Zn containing Al-based alloys has been found to exhibit superior friction and wear properties as well as suitable mechanical properties [5, 7]. The superior tribological properties of zinc-containing aluminum alloys are based on their multiphase microstructures consisted of hard and soft phases, zinc oxides formed on the surface and the properties of the lattice parameter [8, 9]. The hard phases in their microstructures act as load-bearing, while the soft phases facilitate sliding. Zinc oxides were formed by the effect of pressure and temperature in especially dry friction conditions, acting as solid lubricant, facilitate sliding. In addition, it is known that zinc has a hexagonal closed packed (hcp) lattice structure with a high c/a ratio of lattice parameters [10, 11] and is therefore

✉ Şenol Bayraktar
  senol.bayraktar@erdogan.edu.tr

1 Department of Mechanical Engineering, Faculty
   of Engineering, Recep Tayyip Erdogan University, Zihni
   Derin Campus, 53100 Rize, Turkey

easily deformed [12, 13]. This facilitates the movement of the surfaces by reducing the friction forces. It is also known that Zn additions to Al-based alloys improve damping capacity of these alloys as well as mechanical and tribological properties [14, 15]. Their superior hardness, mechanical, tribological and damping properties led to successful use of Zn containing Al-based alloys in practical applications and commercialization of these alloys. There are many commercial aluminum alloys classified as Zamak, ZA and ALZEN series alloys, containing high zinc content (65–95 wt%) [1, 16]. However, in recent years, studies on Al-Zn-based alloys have focused on the development of Al–Zn alloys containing less zinc to reduce their density. The studies carried out for this purpose resulted in the development of a large number of Al–Zn-based alloys [17–19] with different chemical composition containing 5%–35% Zn [20, 21]. Current studies [7, 9] have focused on investigating the usability of these alloys to replace conventional bearing materials such as bronze and white metal. In bearing manufacturing, machining operations such as drilling and milling is one of the most important operation because they are the most effective process on dimension, tolerance, surface integrity and roughness of the final product [22, 23]. These characteristics of the final products vary depending on many parameters. The most important of parameters are the microstructure, hardness, mechanical and tribological properties of the alloy and the properties of the tool used in machining [24, 25]. The effect of different Zn contents on the structural, hardness, mechanical, and tribological properties of Al–Zn alloys is investigated in detail [4, 5]. However, no studies have been conducted showing the effect of Zn content and tool coating on the machining characteristics of Al–Zn bearing alloys. Therefore, it is aimed to investigate the effects of different Zn contents on machinability properties of the Al-(5–35)Zn alloys in detail in this study.

2 Material and Method

Al-5Zn, Al-15Zn, Al-25Zn and Al-35Zn alloys containing 5, 15, 25 and 35 wt% Zn, respectively were produced by permanent mold casting. High purity (99.90%) aluminum and zinc were used in the production of the alloys. Alloying elements were melted in a medium frequency induction melting furnace and cast at temperatures of 650–700 ℃ into conical shape SAE 8620 steel mold under room conditions. Technical drawing of the mold and alloy ingots obtained from this mold are given in Fig. 1. The parts of the ingot where samples are extracted is given in Fig. 1b. The cooling rate during solidification is measured as approximately 0.04 ℃ s^{-1}. Chemical compositions of the produced alloys were analyzed by inductively coupled plasma–optical emission spectrometry (ICP–OES) technique. The microstructural
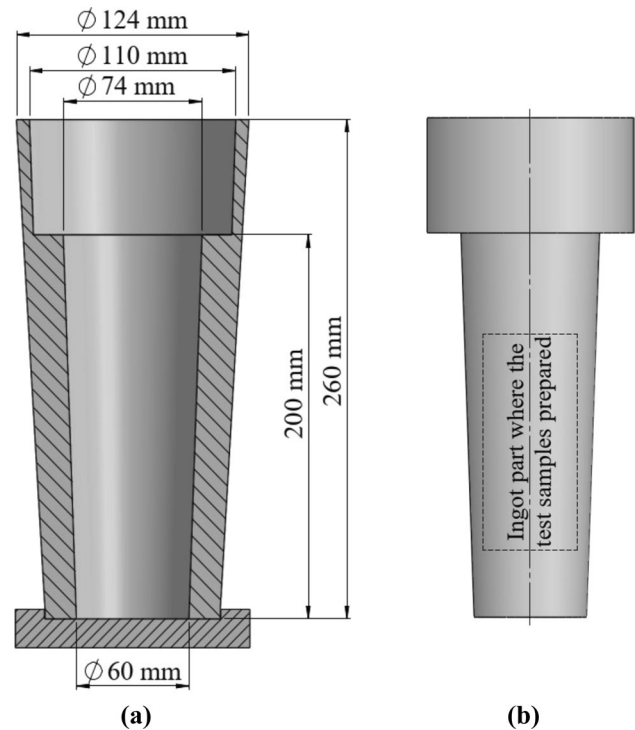

Fig. 1 Technical drawing of the **a** mold used in the castings and **b** alloy ingots obtained from the mold

investigations were performed on samples prepared by standard metallographic methods. Micrographs showing the microstructures of the alloys were obtained using scanning electron microscope (SEM) with backscatter mode. Analysis of the phases in the microstructure of the experimental alloys was made by energy dispersive spectroscopy (EDS) and X-ray diffraction (XRD) methods. EDS studies for α and η phases were carried out by performing multiple analyses on different parts of these phases. In the EDS studies, minimum and maximum amount of alloying elements in the phases was determined. XRD analyses were performed at 20°–90° scan range using a Cu-Kα radiation source with a scan rate of 3° min^{-1} on flat samples and a wavelength of 1.54059 Å. Hardness measurements were carried out with Brinell hardness measurement method by using 2.5 mm diameter indenter under 62.5 kg × f load. Tensile tests were performed with the alloy samples having the diameter and gauge length of 8 × 40 mm at a strain rate of 10^{-3} s^{-1}. Hardness and tensile tests of the alloys were performed with at least six different samples and the values of hardness, tensile strength and elongation to fracture were determined by taking the arithmetic mean of the measured values.

The cutting properties of the alloys were investigated using the 7.5 kW Johnford-VMC 850 CNC vertical machining center. Technical drawing of the workpieces and schematic illustration of the machining center used in the cutting tests are given in Fig. 2. The tests were carried out at a
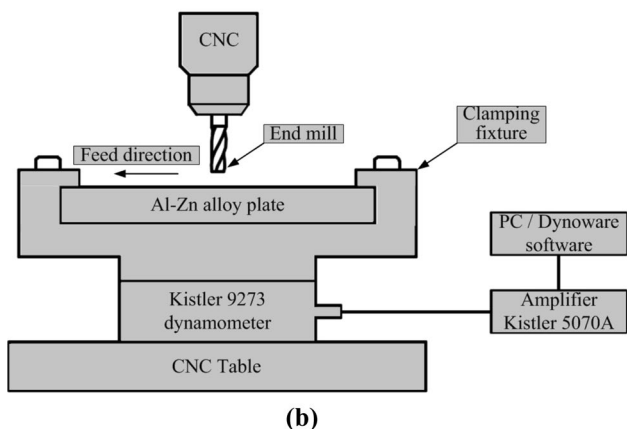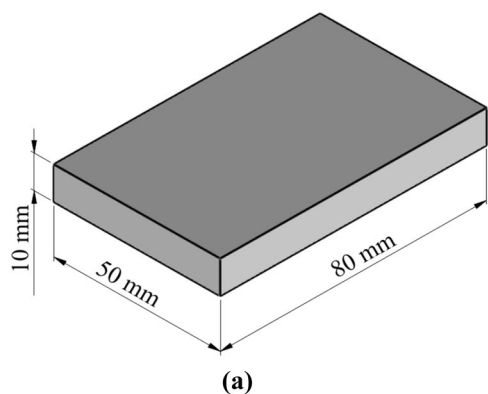
Fig. 2 **a** Technical drawing of the workpieces and **b** Schematic illustration of the machining center used in the cutting tests

constant cutting speed (1200 rev min⁻¹), feed rate (0.1 mm/tooth) and depth of cut (1.5 mm) with both WC and TiAlN coated WC end mills. The technical specifications of these cutting tools obtained from the manufacturer (Sandvik Coromant) are given in Table 1.

The Kistler 9273 model dynamometer and amplifier were used to measure the cutting forces generated during milling of the workpiece. The cutting test results were obtained graphically with Kistler-Dynoware software. The cutting force was considered as a resultant force in the X, Y and Z axes. Mahr Perthometer M1 (MarSurf PS1) brand tracker tip was used for surface roughness measurements. The roughness (Ra) of the machined surfaces was measured in

accordance with ISO 4287. The sampling and measurement lengths were taken as 0.8 mm and 4 mm, respectively, in these measurements. The roughness values of the machined surfaces were calculated by taking the arithmetic mean of the deviations in the surface profile. Three tests were performed for each cutting tool and the shear force and surface roughness values were calculated by taking the arithmetic mean of the results obtained from these experiments.

3 Results and Discussion

ICP–OES analysis results showing the chemical compositions of the produced alloys are given in Table 2.

The micrographs and XRD patterns showing the phases of the alloys tested are given in Figs. 3, 4, 5 and 6, EDS analysis results of the phases observed in the microstructure of the alloys are given in Table 3. These micrographs show that the Al–Zn alloys containing zinc up to 15% exhibit a single-phase microstructure consisting of aluminum rich α-phase (solid solution), Figs. 3 and 4. When the zinc content exceeds 15%, zinc-rich η phase is formed in the microstructure of the alloys in addition to the α phase, Figs. 5 and 6. The formation of these phases in the microstructure of binary Al–Zn alloys has been revealed in previous studies [4, 5] in the based on solidification and solid solubility mechanisms.

The curves showing the change of hardness, tensile strength, and elongation to fracture values of the alloys tested with zinc content are given in Fig. 7. These curves show that the hardness and tensile strengths of the alloys increased with the increasing zinc ratio, but the values of elongation to

Table 2 Chemical composition of the tested alloys

Alloy	Element (wt%)		
	Al	Zn	Impurity elements (Fe, P, V, Zn, Zr, Cu, Mn, Ni, etc.)
Al-5Zn	94.7	5.1	0.2
Al-15Zn	84.7	15.0	0.3
Al-25Zn	74.7	25.2	0.1
Al-35Zn	64.7	35.1	0.2

Table 1 Technical specifications of the cutting tools

Cutting tool	Helix angle (°)	Diameter (mm)	Number of flute	Cutting length (mm)	Coefficient of friction	Coating method	Coating hardness (HV)	Coating thick (µm)
WC end mill	30	6	2	19	> 0.35	–	–	–
TiAlN coated WC end mill					0.3–0.35	PVD (900 ℃)	3300	3
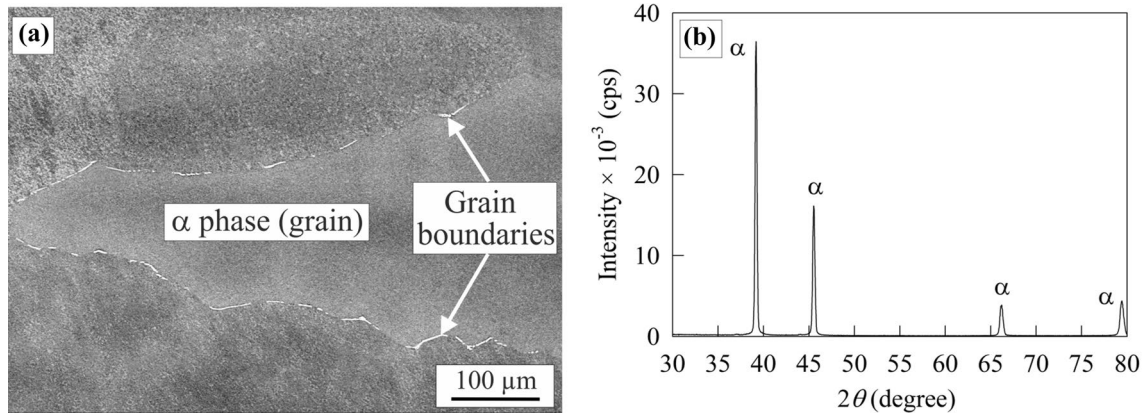
Fig. 3 **a** The micrograph and **b** XRD pattern of the Al-5Zn alloy
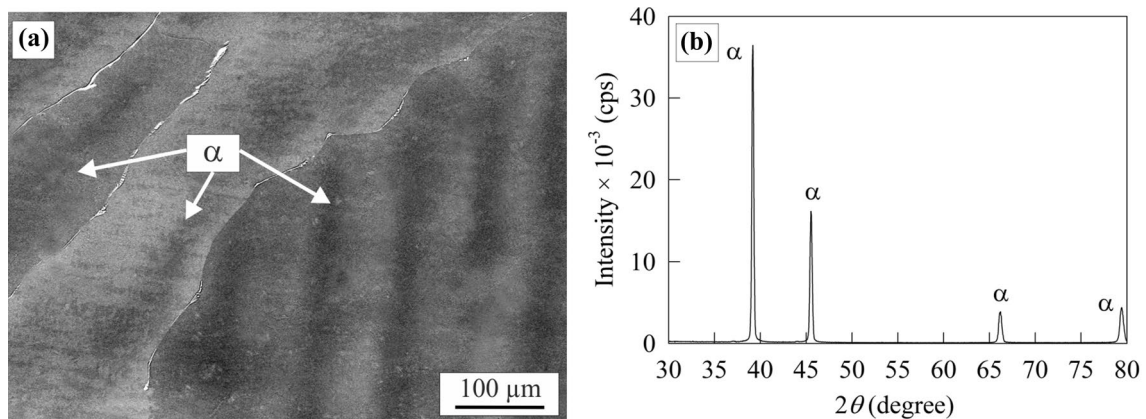

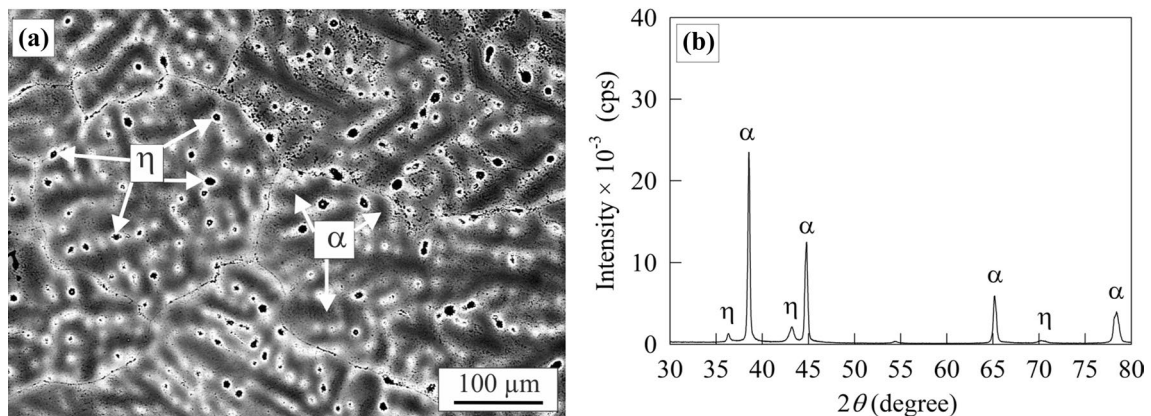**Fig. 4** **a** The micrograph and **b** XRD pattern of the Al-15Zn alloy

Fig. 5 **a** The micrograph and **b** XRD pattern of the Al-25Zn alloy

fracture decreased. The increase in the hardness and tensile strength values of the alloys with the increasing zinc content is explained in the literature [4, 5, 16] in terms of the prevention of dislocations of solid solution hardening and secondary phase precipitation hardening mechanisms. Since

Al-5Zn and Al-15Zn alloys exhibit a single-phase microstructure (α solid solution), only solid solution hardening mechanism is effective in these alloys. However, secondary phase precipitation hardening mechanism can be considered as well as solution hardening mechanism in the Al-25Zn and
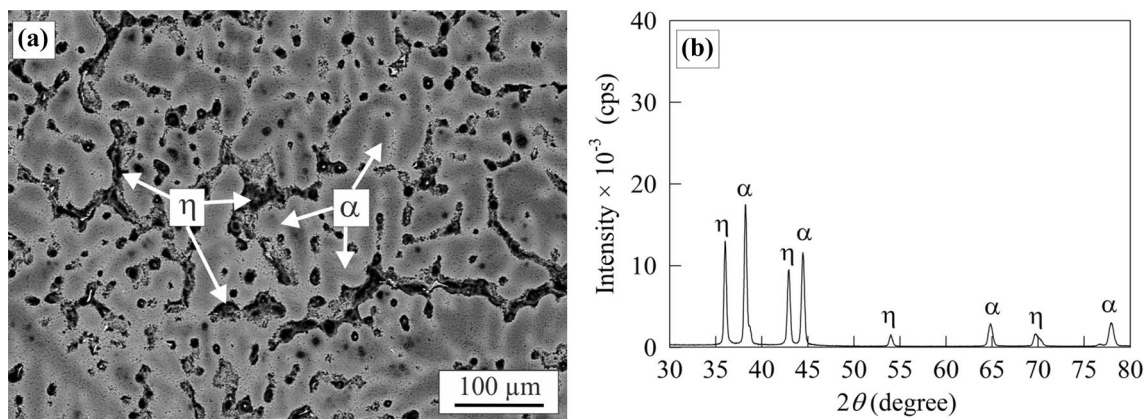
Fig. 6 a The micrograph and **b** XRD pattern of the Al-35Zn alloy

**Table 3** Chemical compositions of the phases in the microstructure of the tested alloys

Alloy	Phases	Chemical compositions (wt%)	
		Al	Zn
Al-5Zn	α	95 ± 1	5 ± 1
Al-15Zn	α	85 ± 1	15 ± 1
Al-25Zn	α	80 ± 3	20 ± 3
	η	3 ± 2	97 ± 2
Al-35Zn	α	79 ± 2	21 ± 2
	η	4 ± 2	96 ± 2

Al-35Zn alloys because these alloys exhibited two phase (α and η) microstructures, Figs. 5 and 6. It was thought that solid solution hardening mechanism is effective up to ~ 20 wt% Zn ratio in the Al-(5–35)Zn alloys because the solubility of Zn in the α phase reached up to ~ 20 wt% with the

increasing zinc content, Table 3. Increase in the strength due to solid solution is expressed by the formula of $\Delta\sigma = A(c)^{1/2}$ [26]; where $\Delta\sigma$ is increase in strength, A is a constant that depends upon the solute–solvent combination and c is the solute concentration (in atomic fraction). According to this equation, solid solution hardening effect depends on solute concentration. Therefore, the effect of solid solution hardening mechanism on Al–Zn alloys is thought to be limited to ~ 20 wt% Zn content. After 20 wt% Zn, it can be said that the secondary phase precipitation is more effective mechanism on the increase in hardness and strength since the zinc content dissolved in the α phase remains approximately constant, Table 3. It is known that the decrease in the elongation to fracture in the Al–Zn alloys [37–38] as the zinc ratio increases is due to forming of the zinc-rich η phase known to be more brittle than aluminum [4, 27].

The curves showing the change of the cutting force values with the zinc content are given in Fig. 8. These curves show that the cutting force is decreased with the increasing zinc

Fig. 7 The variations in hardness, tensile strength and elongation to fracture of Al-(5–35) Zn alloys with zinc content
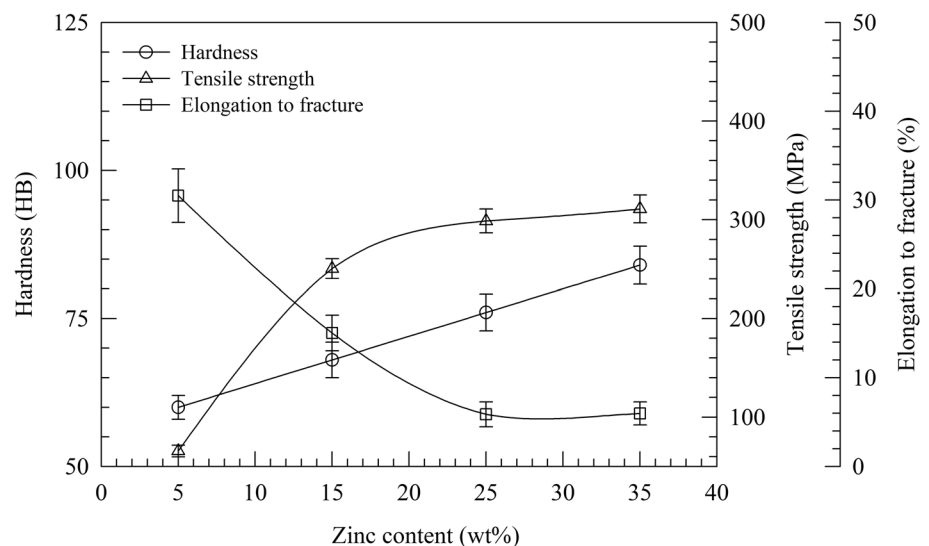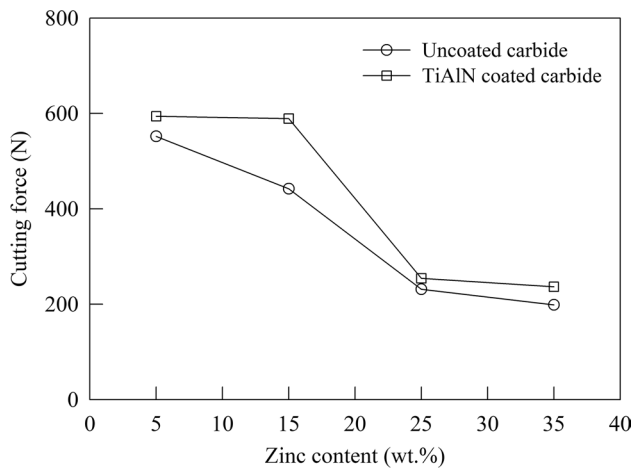
Fig. 8 The change in cutting force of Al-(5–35)Zn alloys with zinc content

content. The decrease in the cutting force with increasing zinc content can be due to the decrease in shear force that acts along the shear plane between the work pieces and chip, and frictional forces between tools and work pieces. Relation between cutting force (F_c) and shear force (F_s) is defined

by a formula of $F_c = (F_s + F_t \times Sin\varphi)/Cos\varphi$, where φ is angle of the shear plane with the surface of work piece and F_t is thrust force [28]. Decrease in shear force required for plastic deformation may be resulted from the properties of crystal structure of Zn. It is reported in the literature that zinc has a hcp crystal structure having a higher c/a lattice parameter ratio than ideal hcp, and therefore, it easily deforms [12]. This leads to a reduction in the shear force required for deformation in Al–Zn alloys as the zinc content increase. It is also known that the Zn rich η phase in the microstructure of the alloys, besides its easy deformation property, acts as a solid lubricant and facilitates sliding [29]. As the zinc content increases, the increase in solid lubricant effect between tools and work pieces may have caused the cutting force to decrease. Decrease in elongation to fracture values with increasing zinc content may also contribute to reducing in cutting force. Decrease in the elongation to fracture of the tested alloys means a reduction in ductility. Reduction of ductility results in a reduction in the amount of material adhering or smearing to the cutting edge of the tool and chip sizes. Less smearing material on the cutting edge and small chip size cause the contact area between the tool and work piece and/or chip to decrease. Since the decrease in the contact areas results in a reduction of frictional forces,
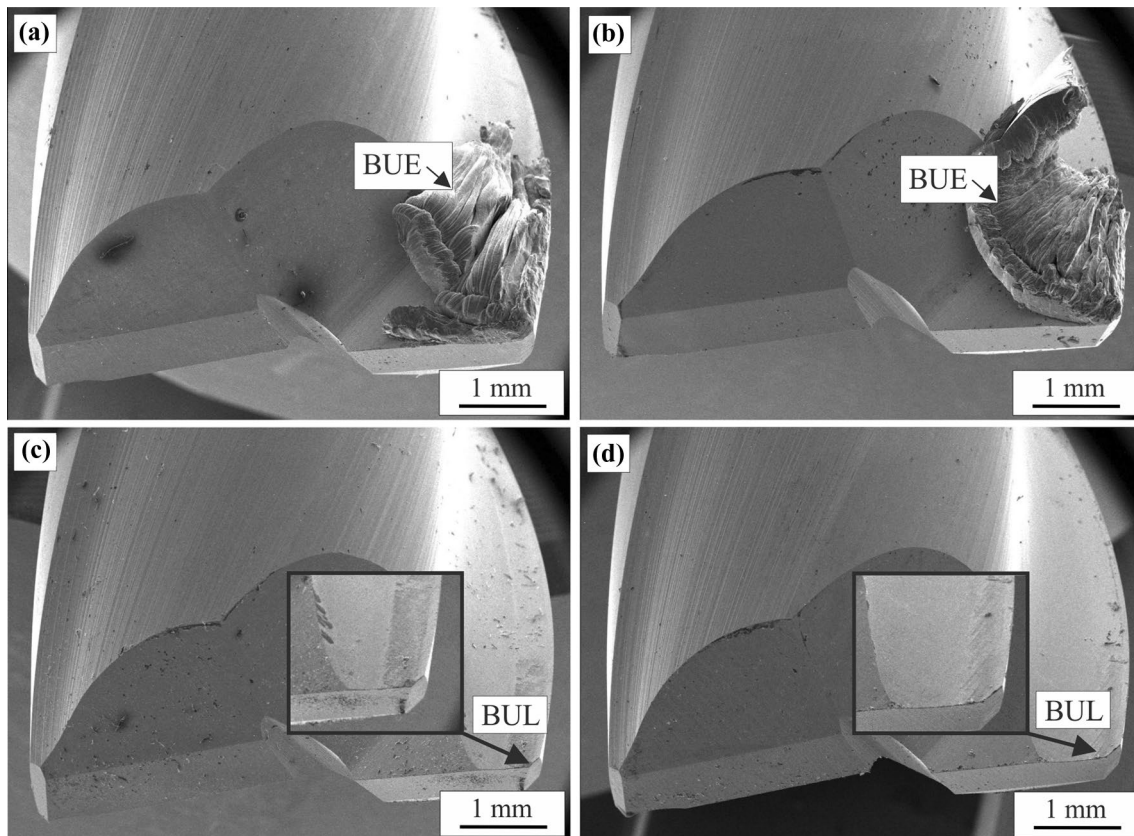

Fig. 9 SEM photographs obtained from WC end mill after cutting, **a** Al-5Zn, **b** Al-15Zn, **c** Al-25Zn and **d** Al-35Zn
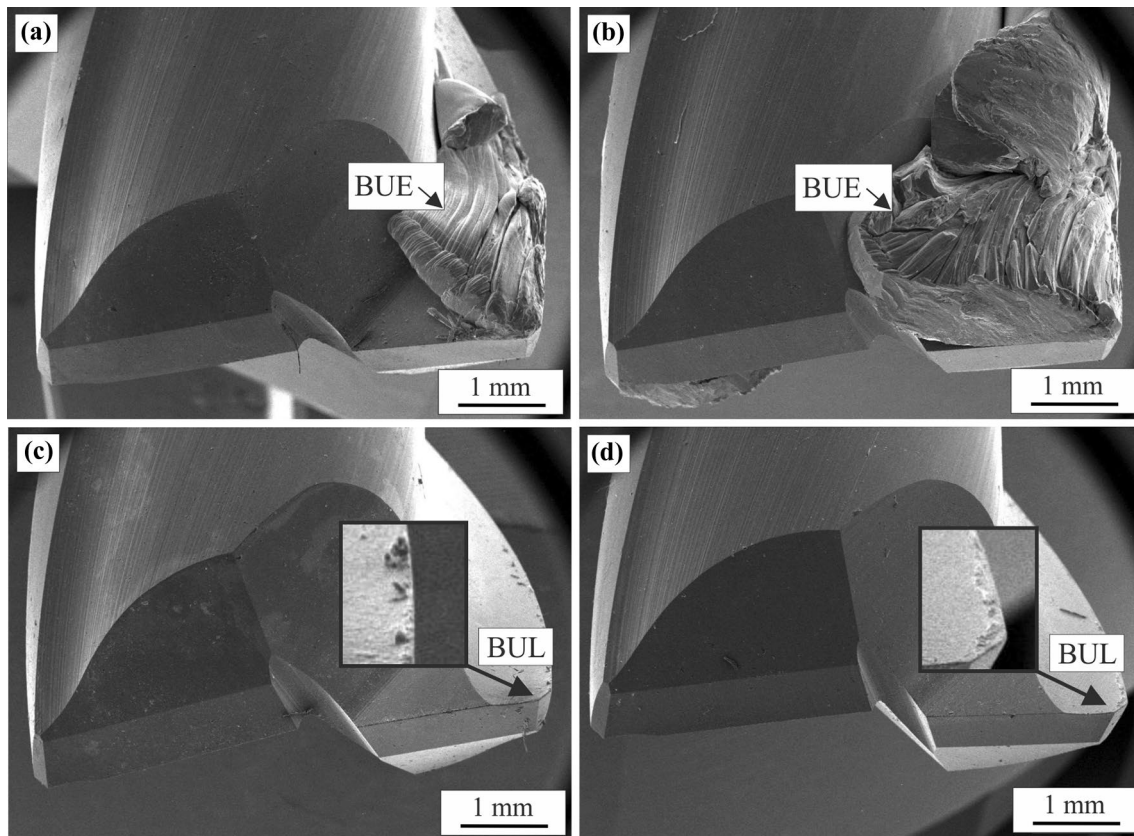
Fig. 10 SEM photographs obtained from TiAlN coated WC end mill after cutting, **a** Al-5Zn, **b** Al-15Zn, **c** Al-25Zn and **d** Al-35Zn
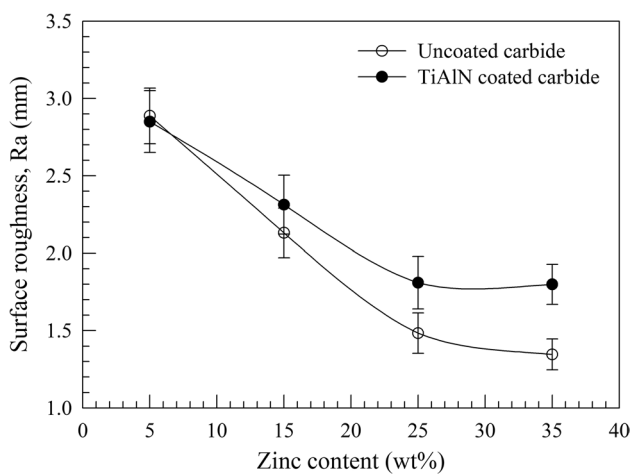

Fig. 11 The curves showing the variations in surface roughness values of the Al-(5–35)Zn alloys with zinc content

cutting forces are expected to decrease [30]. In addition, due to the increase in zinc content, facility of the formation of zinc oxide in the cutting zone may have caused a decrease in cutting force. It is known that zinc oxides are easily formed in the surfaces of zinc-containing materials, especially in the case of dry friction, and these oxides act as solid lubricants and reduce frictional forces [13, 31]. This reduce in frictional forces between tools and work pieces also causes a decrease in cutting force.

The cutting forces in the tests carried out with TiAlN coated WC tools were observed to be higher than the uncoated WC tools, Fig. 8. This may be originated from more material smearing to the TiAlN coated tools during the machining, Figs. 9 and 10. It is thought that more material smearing to the TiAlN coated tools is due to the fact that TiAlN coated WC cutting tools have a lower thermal conductivity coefficient (~ 15 Wm^{-1} K^{-1}) than the uncoated WC tools (~ 40 Wm^{-1} K^{-1}) [32]. It is known that as the thermal conductivity coefficient of the cutting tool decreases, the transfer of the heat generated of the cutting tool-chip interface becomes more difficult and consequently the temperature of the tool, chip, and workpiece increases [33]. Temperature increment in the cutting zone results in a more ductile behavior of the material. Increase in ductility results in both more material adherence to the cutting edge (built up edge-BUE) and forming of continuous chip during cutting, causing increment in tool-work piece and/or chip contact
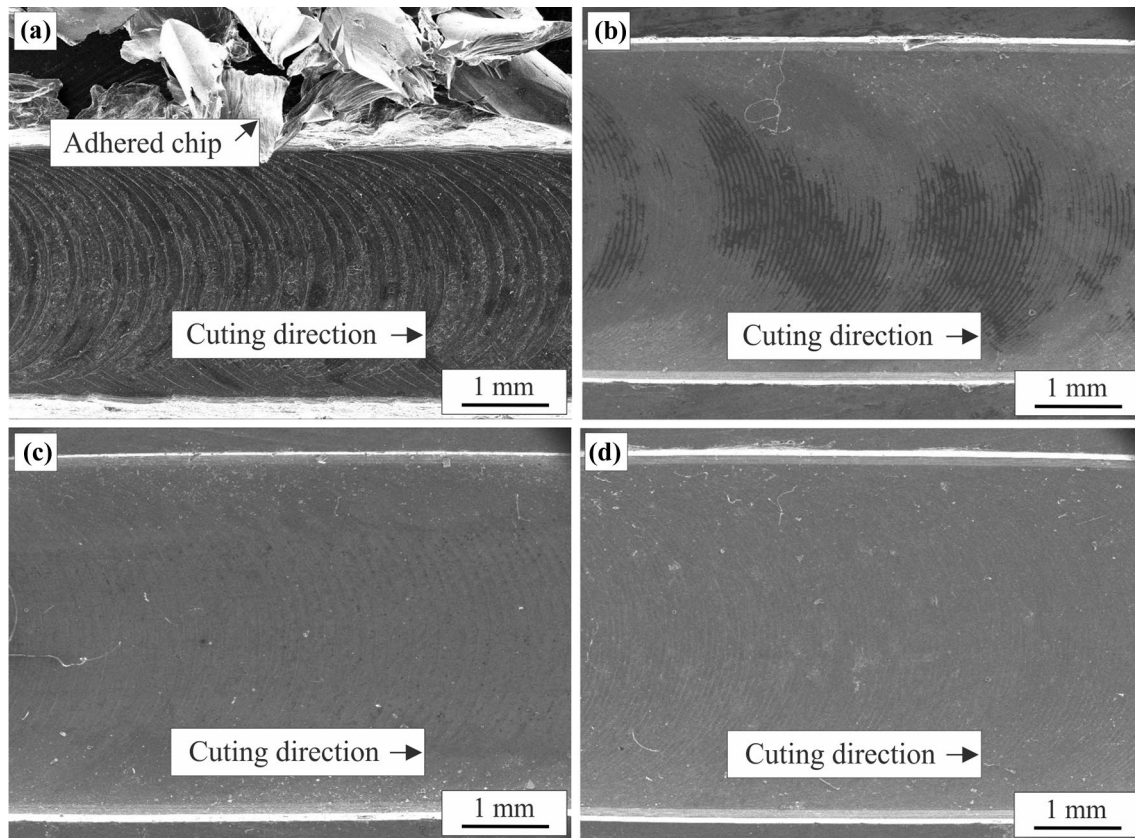
Fig. 12 SEM photo showing the surface of the **a** Al-5Zn, **b** Al-15Zn, **c** Al-25Zn, and **d** Al-35Zn alloy machined with WC end mills

surface area. The increase in contact surface area (A_s) leads to an increase in the shear force (F_s) required to exceed the shear stress value (τ) of the material. In the literature [28], the relationship between these parameters is defined by the formula $\tau = F_s/A_s$, and according to this equation, as the A_s value increases, the F_s value required for the deformation must increase. Increase in the F_s also causes increases in the cutting force (F_c) according to the $F_c = (F_s + F_t \times \sin\varphi)/\cos\varphi$ formula given above.

SEM photographs obtained from cutting tools after cutting are given in Figs. 9 and 10. These photographs show that BUE and BUL are formed on the cutting surface of the cutting tool, but the BUE and BUL formation decreases as the zinc content increases. These photos also show that more BUE and BUL are formed in the surfaces of the TiAlN coated tools. It is known that BUE and BUL occur as a result of accumulation of heavily deformed work material on the cutting edge under proper conditions [34, 35]. BUE occurs on the cutting edge of the tool, while BUL is formed along the cutting edge surface of the tool [36]. It is also known

that formation of a built-up edge and its stability connect with the coefficient of sliding friction between the cutting tool and the flowing chip and it is believed that the origin of a built-up edge and its stability are linked with this coefficient of friction, which increases at first as the temperature increases [37, 38]. The decrease in the BUE and BUL formation as the zinc ratio increases may be due to the characteristic of the lattice structure of the zinc, decrease in ductility, and the zinc oxides formed between the contacting surfaces. The reduction in ductility can facilitate the removal of the chip from the cutting environment and prevent the chip from sticking to the tool. In addition, the property that zinc has a hcp lattice structure and the c/a lattice parameter ratio is high causes to facilitate sliding in zinc-containing alloys and to reduce friction. It is also known that zinc oxides form in the contacting surfaces of the zinc-containing alloys under dry (unlubricated) sliding conditions, which reduces the friction by acting as solid lubricant. Reducing the friction between the tool and workpiece due to this material features results in decrease in the formation of BUE and BUL
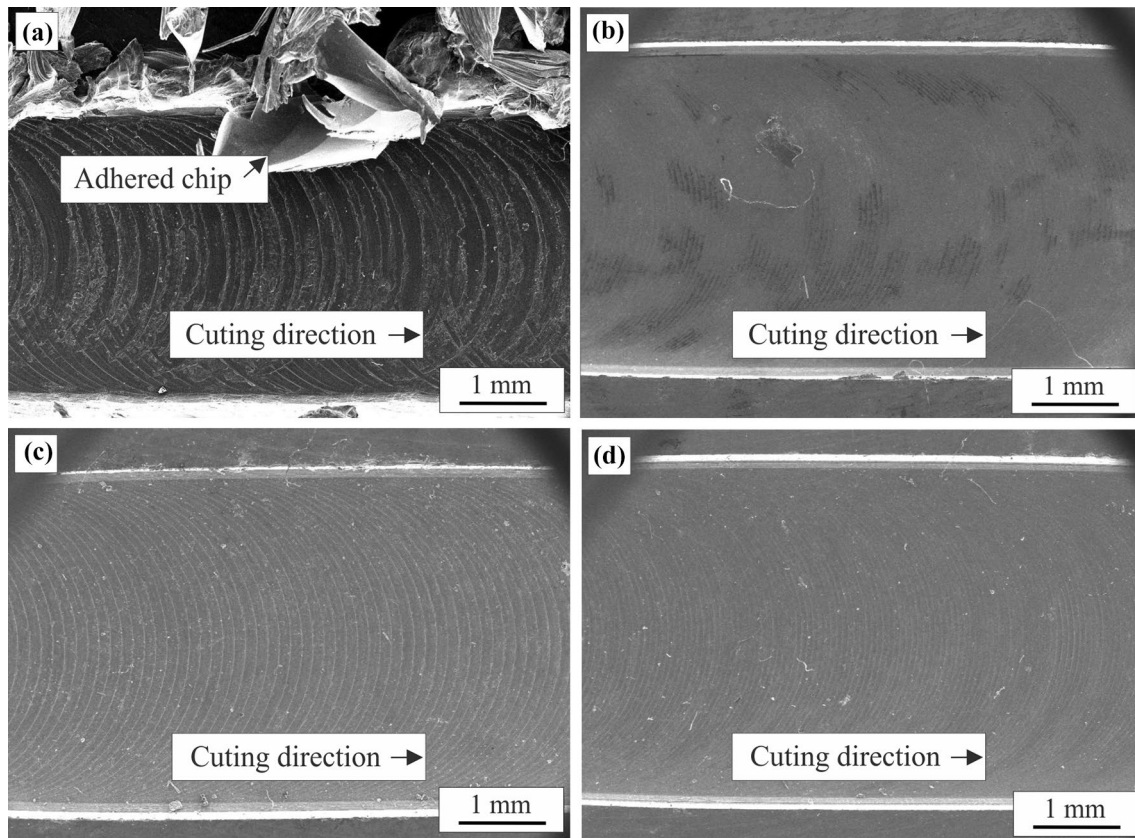
Fig. 13 SEM photo showing the surface of the **a** Al-5Zn, **b** Al-15Zn, **c** Al-25Zn, and **d** Al-35Zn alloy machined with TiAlN coated WC end mills

with the increasing zinc content [39]. More BUE and BUL observed in TiAlN-coated tools may be due to increased chip and work piece ductility due to more heat accumulation in the cutting zone. It is known that the increase in ductility increases the friction between the tool and the chip, thus facilitates the seizure mechanism [40].

The curves showing the change of surface roughness values of the machined surfaces with zinc content are given in Fig. 11 and SEM images of the machined surfaces are given in Figs. 12 and 13. Figure 11 shows that surface roughness values of the tested alloys decreased with increasing zinc content. This may be due to the increase in zinc content, the easier deformation of roughs in the surface, easier removal of chips, and improved cutting quality due to less smeared material (BUE and BUL) in the cutting edge of end mill. The easier deformation (shaping) of the roughs on the surfaces with increasing zinc content is due to the mentioned above

property of the high c/a ratio of hcp crystal structure of zinc. It is thought that the easier removal of the chips from the cutting environment with the increased zinc content is due to the decrease in elongation to fracture. In case of decreasing elongation to fracture, the removal of the chips from the surface becomes easier and the smearing is reduced. This leads to a reduction in irregularities on the surface of the workpiece and to an increase in surface quality. The quality of the machined surface also increases with decreasing BUE and BUL formation on the cutting tools [41]. The built-up edge causes periodically break off and reforms, introducing irregularities into the surface [42]. Therefore, reduction or non-occurrence of irregularities increases the surface quality. In addition, zinc oxides likely to be formed between the surfaces of the tool and the workpiece may act as solid lubricants during friction. This may have contributed to the
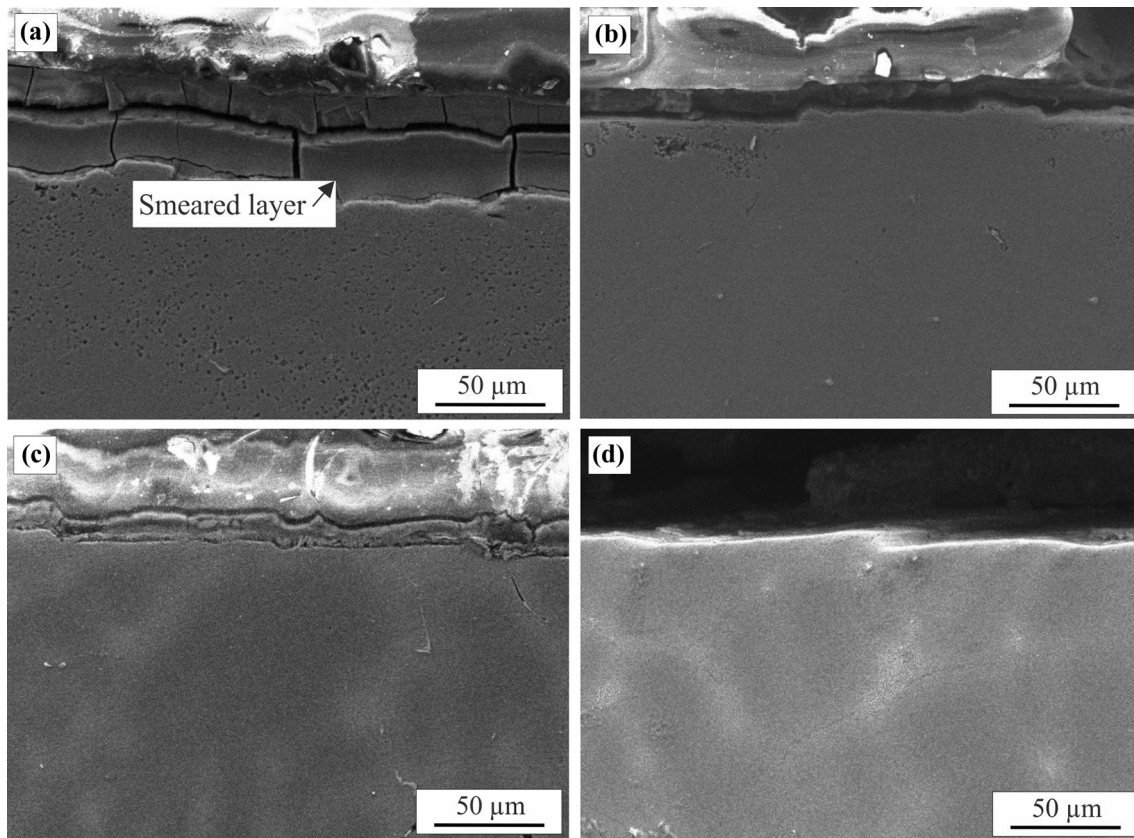
Fig. 14 SEM micrograph showing the subsurface of the **a** Al-5Zn, **b** Al-15Zn, **c** Al-25Zn, and **d** Al-35Zn alloy sample machined with WC end mills

reduction of frictional forces and thus to an increase in surface quality.

The surface roughness values of the samples machined with the TiAlN coated tools and chip amount on the surface were observed higher than the surfaces machined with the uncoated tools, Figs. 11, 12 and 13. This observation can be explained by the BUE and BUL mechanisms, as well as by changes in the heat conduction coefficient and geometry of the cutting tool due to the coating. It is known that the contact surface area between the cutting edge of the coated tools and the workpiece is greater than the uncoated tool [43]. It was also observed that more BUE and BUL formed in coated tools compared to uncoated tools, Figs. 9 and 10. The increase in the contact area between the tool and workpiece due to change in the tool geometry and increase in the BUE and BUL formation causes an increase in the cutting force [44]. This results in increased friction heat. More

heat accumulates on the tool, workpiece and chip during the machining with coated tools, as both more friction is occurred and the heat conduction coefficient of coated tool is lower than the uncoated tool. Accumulating heat due to lower heat conduction coefficient increases the ductility of the chip, which facilitates smearing of it on the tool. Both the smeared material and the ductile chip can adhere to the surface of the workpiece again during the cutting process due to the effect of cutting pressure and temperature. This can lead to an increase in surface roughness, in other words, to a decrease in the quality of the treated surfaces.

Subsurface photographs showing the changes occurring on both the surface layer and under the machined surface of the samples are given in Figs. 14 and 15. These photos show that a smearing layer is formed on the surfaces of Al–Zn alloys after the cutting. Such layers in Al–Zn alloys are known to occur as a result of chips or wear particles
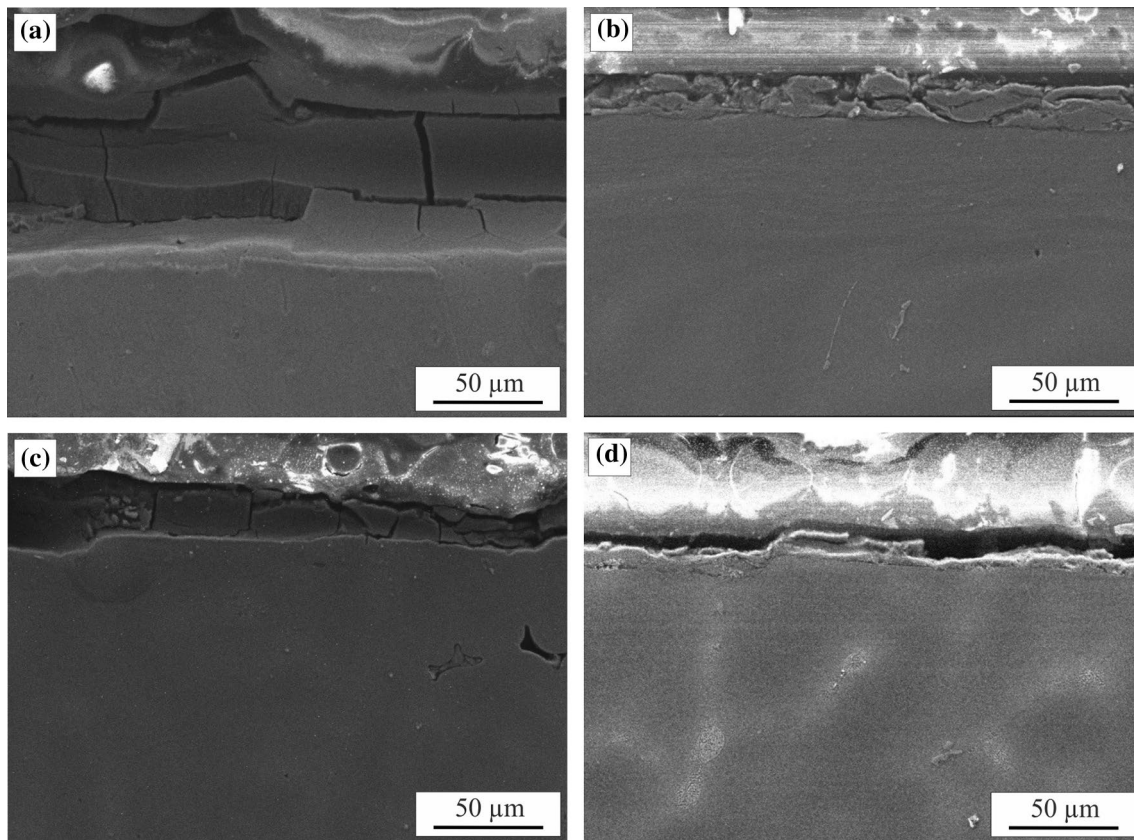
Fig. 15 SEM micrograph showing the subsurface of the **a** Al-5Zn, **b** Al-15Zn, **c** Al-25Zn, and **d** Al-35Zn alloy sample machined with TiAlN coated WC end mills

re-adhered to the surface due to pressure and temperature [45]. The thickness of this smeared layer decreased with increasing zinc content, Figs. 14 and 15. This can be due to the fact that zinc is easily removed from the cutting zone due to its low ductility. On the surfaces of Al–Zn alloy samples machined with TiAlN coated tools, a thicker smeared layer was formed than the samples machined with uncoated WC tools. This can be due to the higher ductility of the chip due to more heat accumulation in the cutting zone.

The photographs showing the chip characteristics of Al-(5–35) Zn alloys are given in Figs. 16 and 17. The chip forms can be classified as Type 2 for Al-(5–15) Zn alloys and Type 2 for Al-(25–35)Zn alloys according to the chip classification made by Ernst [46] Type 3 is continuous chip with built-up edge adjacent to the tool face. This chip type is commonly encountered in ductile materials. Surface finish

is rough due to fragments of built-up edge escaping with the work piece. This is confirmed by tool photos (Figs. 9a, b, 10a, b), surface roughness values (Fig. 11) and surface photos (Figs. 12a, b, 13a, b). Type 2 is continuous chip with continuously escaping compressed layer adjacent to the tool face. According to Ernst, this chip type is the ideal chip form for the quality of machined surface finishing, temperature of the tool point and power consumption. The formation mechanisms of these types of chips are described in detail in the literature [46]. The change in the chip type and the decrease in the amount of chip adhering to the tool can be due to the decrease in the ductility of the alloy with the increased zinc ratio. It was observed that cross-sectional area of the chips decreased with increasing zinc content, Figs. 16 and 17. It was also observed that the chips obtained in the cutting tests carried out with uncoated cutting tools were smaller than
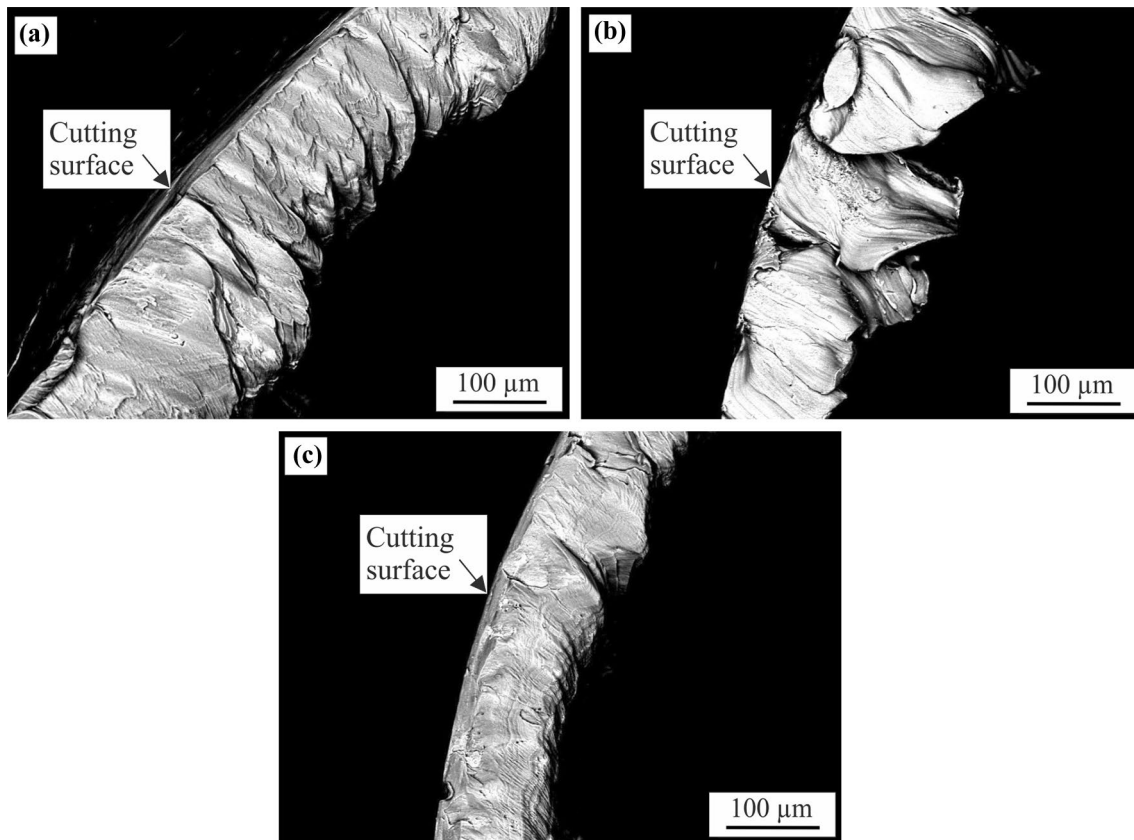
Fig. 16 SEM micrograph showing the chip characteristics of the **a** Al-15Zn, **b** Al-25Zn, **c** Al-35Zn, and **d** Al-35Zn alloy machined with WC end mills

those in the tests carried out with the TiAlN coated cutting tools, Figs. 16 and 17. Smaller chips may be the result of less ductility. It is known that the chip compression ratio decreases with the decreasing ductility and therefore the chips are small as the ductility decreases [47].

4 Conclusions

In this study, the effect of zinc content and tool coating on the machinability of Al-(5–35)Zn alloys having high aluminum content was investigated experimentally. It was observed that the increasing zinc addition positively affect the machinability properties of Al–Zn alloys while TiAlN coated tools negatively affected. The conclusions drawn from the present work are given below.

(1) Al-(5–15)Zn alloys exhibit single phase (Al rich-α) microstructure while Al-(25–35) alloys exhibit two phase (Al rich-α and zinc rich η) microstructure.
(2) Increased zinc content leads to an increase in hardness and strength in Al-(5–35)Zn alloys, while reducing elongation to fracture.
(3) The cutting force, surface roughness, chip size and formation of the BUE and BUL during the machining of the Al-(5–35)Zn alloys decrease with increasing zinc content.
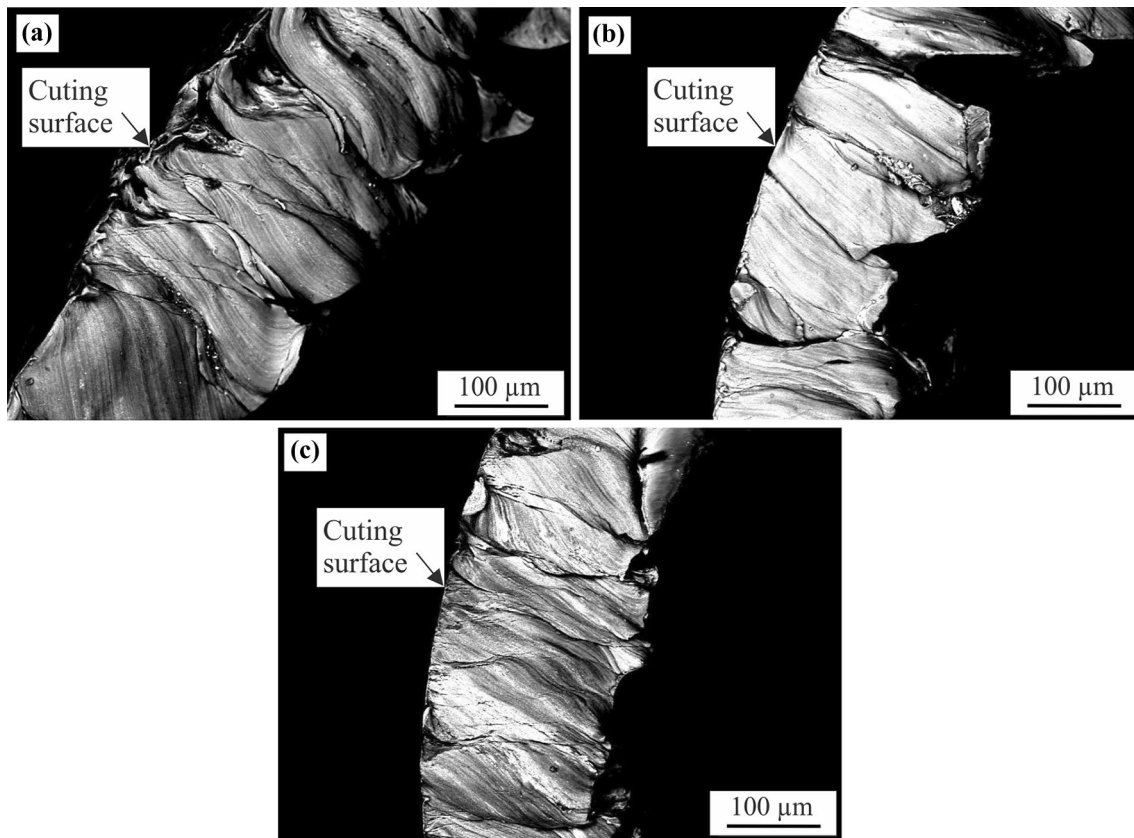
Fig. 17 SEM micrograph showing the chip characteristics of the **a** Al-15Zn, **b** Al-25Zn, **c)** Al-35Zn, and **d** Al-35Zn alloy machined with TiAlN coated WC end mills

(4) The machining of the Al-(5–35)Zn alloys with WC tools needs lower cutting force and surface roughness compared to the machining with TiAlN coated WC tools.

(5) The machining of the Al-(5–35) alloys with WC tools results in higher surface quality compared to the machining with TiAlN coated tools.

Compliance with Ethical Standards

Conflict of interest The authors declare that they have no conflict of interest.

References

1. R.J. Barnhurst, *Zinc Aluminum Alloy Design; Manual for Continuous Rotation Bearings* (Noranda Research Centre, Canada, 1998)

2. T. Savaskan, Y. Alemdağ, Effect of nickel additions on the mechanical and sliding wear properties of Al-40Zn-3Cu Alloy. Wear **268**(3–4), 565–570 (2010)

3. T. Savaşkan, A.P. Hekimoğlu, Relationships between mechanical and tribological properties of Zn-15Al-based ternary and quaternary alloys. Int. J. Mater. Res. **107**(7), 646–652 (2016)

4. A.P. Hekimoğlu, Y.E. Turan, Effect of zinc content on the microstructure and mechanical properties of the Al-(5-50)Zn alloys. Gümüşhane Uni. J. Sci. Tech. Inst. **9**(1), 16–25 (2019)

5. T. Savaşkan, O. Bican, Y. Alemdağ, Developing aluminium–zinc-based a new alloy for tribological applications. J. Mater. Sci. **44**(8), 1969–1976 (2009)

6. E.D. George, *Mechanical Metallurgy* (McGraw-Hill, England, 1986)

7. A.P. Hekimoğlu, T. Savaşkan, Lubricated wear characteristics of Zn-15Al-3Cu-1Si alloy and SAE 660 bronze. J. Fac. Eng. Arc. Gazi Uni. **33**(1), 145–154 (2018)

8. B.K. Prasad, Investigation into sliding wear performance of zinc-based alloy reinforced with SiC particles in dry and lubricated conditions. Wear **262**(3–4), 262–273 (2007)

9. A.P. Hekimoğlu, T. Savaşkan, Effects of contact pressure and sliding speed on the unlubricated frictionand wear properties of Zn-15Al-3Cu-1Si Alloy. Tribol. Trans. **59**(6), 1114–1121 (2016)

10. R.A. Donald, P.F. Pradeep, *Essentials of Materials Science & Engineering-SI Version* (Cengage Learning, Canada, 2009)

11. M. Linga, Effect of c/a-ratio on crystallographic texture and mechanical anisotropy of hexagonal close packed metals. Mater. Sci. For. **426–432**(4), 3575–3580 (2003)

12. A.K. Bhargava, C.P. Sharma, *Mechanical Behaviour and Testing of Materials* (PHI learning Private Limited, New Delhi, 2014)

13. D.P. Mondal, S. Das, V. Rajput, Effect of zinc concentration and experimental parameters on high stress abrasive wear behaviour of Al–Zn alloys: a factorial design approach. Mater. Sci. Eng. A **406**(1–2), 24–33 (2005)

14. I.G. Ritchie, Z.L. Pan, F.E. Goodwin, Characterization of the damping properties of die-cast zinc–aluminum alloys. Metall. Mater. Trans. A **22**(3), 617–622 (1991)

15. C.P. Frank, *Zinc Handbook: Properties, Processing, and Use In Design* (Marcel Dekker, North Carolina, 1991)

16. A.P. Hekimoğlu, T. Savaşkan, Structure and mechanical properties of Zn-(5–25) Al alloys. Int. J. Mater. Res. **105**(11), 1084–1089 (2014)

17. S.S. Sang, Y.Y. Gil, Y.K. Tae, M.P. Ik, Microstructure and mechanical properties of TiB-Containing Al–Zn binary alloys. J. Mater. Sci. Technol. **32**(7), 653–659 (2016)

18. A.P. Hekimoğlu, Y.E. Turan, İİ. İsmailoğlu, M.E. Akyolm, E. Şen, Effect of grain refinement with boron on the microstructure and mechanical properties of Al-30Zn alloy. J. Fac. Eng. Arc. Gazi Uni. **18**(1), 1–17 (2018)

19. T. Savaşkan, O. Bican, Dry sliding friction and wear properties of Al-25Zn-3Cu-(0–5)Si alloys in the as-cast and heat-treated conditions. Tribol. Lett. **40**(3), 327–336 (2010)

20. G.K. Manjunath, K.G.V. Preetham, B.K. Udaya, P. Huilgol, Microstructure and mechanical properties of cast Al-5Zn-2Mg alloy subjected to equal-channel angular pressing. J. Mater. Eng. Perform. **27**(11), 5644–5655 (2018)

21. I. Yanxia, L. Ping, Z. Gang, L. Xiaotao, C. Jianzhong, The constituents in Al–10Zn–2.5Mg–2.5Cu aluminum alloy. Mater. Sci. Eng. A **397**(1–2), 204–208 (2005)

22. F.J. Trujillo, L. Sevilla, M. Marcos, Cutting speed-feed coupled experimental model for geometric deviations in the dry turning of UNS A97075 Al-Zn alloys. Adv. Mech. Eng. **6**, 1–11 (2014)

23. B. De Agustina, A. Saá, M. Marcos Bárcena, E.M. Rubio, Analysis of the machinability of aluminium alloys UNS A97050-T7 and UNS A92024-T3 during short dry turning tests. Adv. Mater Res. **264**, 931–936 (2011)

24. B. De Agustina, E.M. Rubio, M. Villeta, M.A. Sebastian, Experimental investigation of dry turning of UNS A97050-T7 aluminium alloy bars based on surface roughness. Int. J Mech. Manuf. Syst. **3**(5–6), 437–450 (2010)

25. F. Trujillo, L. Sevilla, M. Marcos, Experimental parametric model for indirect adhesion wear measurement in the dry turning of UNS A97075 (Al–Zn) alloy. Materials **10**(2), 152 (2017)

26. G.E. Dieter, *ASM Handbook: Materials Selection and Design* (ASM International, Cleveland, 1997)

27. L.F. Mondolfo, *Aluminum Alloys: Structure and Properties* (Butterworth & Co Publishers, London, 1976)

28. M.P. Groover, *Fundamentals of Modern Manufacturing: Materials Processes, and Systems* (Wiley, Hoboken, 2007)

29. B.K. Prasad, Dry sliding wear response of zinc-based alloy over a range of test speeds and loads: a comparative study with cast iron. Trib. Let. **25**(2), 103–115 (2007)

30. J.L. Jorstad, Influence of aluminum casting alloy metallurgical factors on machinability. SAE Trans. **89**(2), 1892–1906 (1980)

31. T. Savaşkan, G. Pürçek, S. Murphy, Sliding wear of cast zinc-based alloy bearing under static and dynamic loading conditions. Wear **252**(9–10), 693–703 (2002)

32. F. Akbar, P. Mativenga, M. Sheikh, Heat partition-based design of hard coatings in high-speed machining. Int. J. Mach. Mach. Mater. **14**(4), 363–386 (2013)

33. D. Dudzinski, A. Molinari, H. Schulz, *Metal cutting and high speed machining* (Kluwer Academic/Plenum Publishers, New York, 2002)

34. J.R. Davis, A.S.M. Handbook, *Machining* (ASM International, USA, 1989)

35. N. Narutaki, Y. Yamane, Tool wear and cutting temperature of CBN tools in machining of hardened steels. Ann. CIRP **28**(1), 23–28 (1979)

36. M.S. Carrilero, J.M.S. Sola, J.M. Sanchez, M. Alvarez, J. Gonzalez, M. Macros, A SEM and EDS insight into the BUL and BUE differences in the turning process of AA2024 Al–Cu Alloy. Int. J. Mach. Tools Manuf. **42**(2), 215–220 (2002)

37. M. Nouari, G. List, F. Girot, D. Coupard, Experimental analysis and optimisation of tool wear in dry machining of aluminium alloys. Wear **255**(7–12), 1359–1368 (2003)

38. M. Nouari, G. List, F. Girot, D. Gehin, Effect of machining parameters and coating on wear mechanisms in dry drilling of aluminium alloys. Int. J. Mach. Tools Manuf. **45**(12–13), 1436–1442 (2005)

39. L.C. Donald, Zinc in aluminum casting alloys. Trans. Am. Found. Soc. **60**, 517 (1952)

40. E. Ezugwu, Z. Wang, Titanium alloys and their machinability—a review. J. Mater. Process. Technol. **68**(3), 262–274 (1997)

41. A. Kamboj, S. Kumar, H. Singh, Burr height and hole diameter error minimization in drilling of Al6063/15%/SiC composites using HSS step drills. J. Mech. Sci. Tech. **29**(7), 2837–2846 (2015)

42. A. David, J.S.A. Stephenson, *Metal Cutting Theory and Practice* (Taylor & Francis Group, London, 2016)

43. A. Rivero, G. Aramendi, S. Herranz, L.L. Lacalle, An experimental investigation of the effect of coatings and cutting parameters on the dry drilling performance of aluminium alloys. Int. J. Adv. Manuf. Technol. **28**(1–2), 1–11 (2006)

44. Y. Zhou, H. Sun, A. Li, M. Lv, C. Xue, J. Zhao, FEM simulation-based cutting parameters optimization in machining aluminum–silicon piston alloy ZL109 with PCD tool. J. Mech. Sci. Tech. **33**(7), 3457–3465 (2019)

45. P. Gençağa, T. Savaşkan, T. Küçükömeroğlu, S. Murphy, Dry sliding friction and wear properties of zinc-based alloys. Wear **252**(11–12), 894–901 (2002)

46. V.P. Astakhov, *Tribology of Metal Cutting* (Elsevier, Amsterdam, 2006)

47. M. Asad, F. Girardin, T. Mabrouki, J.F. Rigal, Dry cutting study of an aluminium alloy (A2024-T351): a numerical and experimental approach. Int. J. Mater. Form. **1**(1), 499–502 (2008)